Photodissociation of N_2O_4 Adsorbed on Amorphous and Crystalline Water−Ice Films

Akihiro Yabushita, Yoshihiko Inoue, Takehito Senga, and Masahiro Kawasaki*

Graduate School of Global Environmental Studies and Department of Molecular Engineering, Kyoto University, Kyoto 606-8501, Japan

Shinri Sato

Catalysis Research Center and Graduate School of Environmental Earth Science, Hokkaido University, Sapporo 060-0811, Japan

Received: September 7, 2003

The photodissociation dynamics of N_2O_4 adsorbed on amorphous and polycrystalline water−ice films has been studied at 193, 248, and 351 nm. The adsorbed states of N_2O_4 on the ice films at 80−140 K were investigated by infrared-absorption and temperature-programmed desorption measurements. Time-of-flight (TOF) spectra of the photofragments were measured by probing the resonance-enhanced multiphoton ionization signals of $NO(v,J)$ and $O(^3P_j)$. Internally and translationally relaxed NO photofragments were observed. Their energy distributions were mostly independent of the states of the ice films and the photolysis laser wavelengths. The TOF distributions of $NO(v = 0)$ consist of fast and slow components. The slow component is dominant. A large difference in the dissociation yields between amorphous and crystalline ice experiments was observed.

Introduction

Photodissociation of molecules adsorbed on, or in, a water−ice film is a new type of heterogeneous photochemistry, which is related to environmental chemistry, astrochemistry, etc. For example, the air-mixing ratio of NO_x in the summer arctic region is high due to photochemical processes of NO_3^- in snow by solar UV flux.[1−3] Complex organic compounds are photochemically produced by the vacuum ultraviolet irradiation on a mixture of methane, ammonia, and carbon monoxide in cosmic ice particles.[4] The mechanism and dynamics of the photodissociation of simple molecules adsorbed on water−ice have been reported for Cl_2,[5] CO,[6] ClO_2,[7,8] Cl_2O,[9] CO_2,[10] NH_3,[11] $CFCl_3$,[12,13] O_3,[14] and NO_2.[15−18] Among them, the photochemistry of NO_2 is not simple because N_2O_4 is the sole species observed on the ice surface when NO_2 molecules are adsorbed from the gas phase to a water−ice film below 140 K.[15,19] Since the desorption enthalpy of N_2O_4 from the ice surface is 39 kJ mol^{-1}, due to the interaction with the ice film surface,[15] the internal energy of the photofragments from N_2O_4 is relaxed when it is photodissociated. Susa and Koda reported the photodissociation of N_2O_4 adsorbed on annealed and nonannealed water−ice film at 193 nm using mass spectrometry.[18] The main products are NO and NO_2 in a 1:1 ratio for the annealed ice and 1:10 for the nonannealed ice. The speed distributions of NO consist of the slow and fast components. The slow component is accommodated to the substrate temperature. They suggested strong interaction between the adsorbate and the ice surface. When N_2O_4 adsorbed on an insulator or a metal substrate is photodissociated at 193 and 248 nm, the NO photofragments are internally excited.[20−22] NO_2 was released at 355 nm, and its translational temperature is as low as the metal substrate temperature.[16,17]

In this work we have studied the UV photodissociation mechanism and dynamics of N_2O_4 adsorbed on amorphous and crystalline water−ice films at 193, 248, and 351 nm in order to investigate the interaction of the adsorbate molecule with water molecules. We have used infrared reflection absorption spectroscopy (IRAS) and temperature-programmed desorption spectroscopy (TPD) for measurement of the surface-adsorbed species on the ice films. We have measured the translational and internal energy distributions of the NO and O atom photofragments with two-photon resonance-enhanced multiphoton ionization (REMPI) and photofragment time-of-flight (TOF) spectroscopy.

Experimental Section

1. Measurement of IRAS at Hokkaido University. IRAS measurements performed in an ultrahigh vacuum system have been described previously.[23] An Au(111) single-crystal substrate placed in the vacuum chamber was cleaned by Ar^+ sputtering at 800 K and annealing at 900 K. Ozone was used for surface cleaning. For IRAS measurements, the IR beam from a FTIR spectrometer (BIO-RAD, model FTS-155, 4 cm^{-1} resolution) was p polarized by a wire grid polarizer and then introduced into the vacuum chamber with the incident angle of the IR beam of 85°.

When water was deposited at temperatures below $T = 100$ K by the backfilling method, a highly porous amorphous ice film was formed on Au(111). This kind of ice film is called a porous−amorphous solid-water (PASW) film. After the film was heated, the IRA spectrum of the ice changed significantly. The bulk OH stretching band shifted to lower frequencies by more than 100 cm^{-1} at 140 K, while the band intensities of both the free OH group and the HOH bending decreased. The spectrum at 140 K was nearly identical to that of crystalline ice.[24] Since these spectral changes started at 120 K, the phase change of PASW to polycrystalline ice (PCI) occurs above 120 K. In this experiment, a PASW film was prepared by deposition of water on Au(111) at <100 K. A PCI film was prepared by annealing the PASW film at 130 K for > 25 min and then cooling to an appropriate temperature. Purified NO_2 gas was deposited by the backfilling method.

---

* Author to whom correspondence may be addressed. E-mail: kawasaki@moleng.kyoto-u.ac.jp. Fax: +81-75-383-2573.

10.1021/jp036670j CCC: $27.50

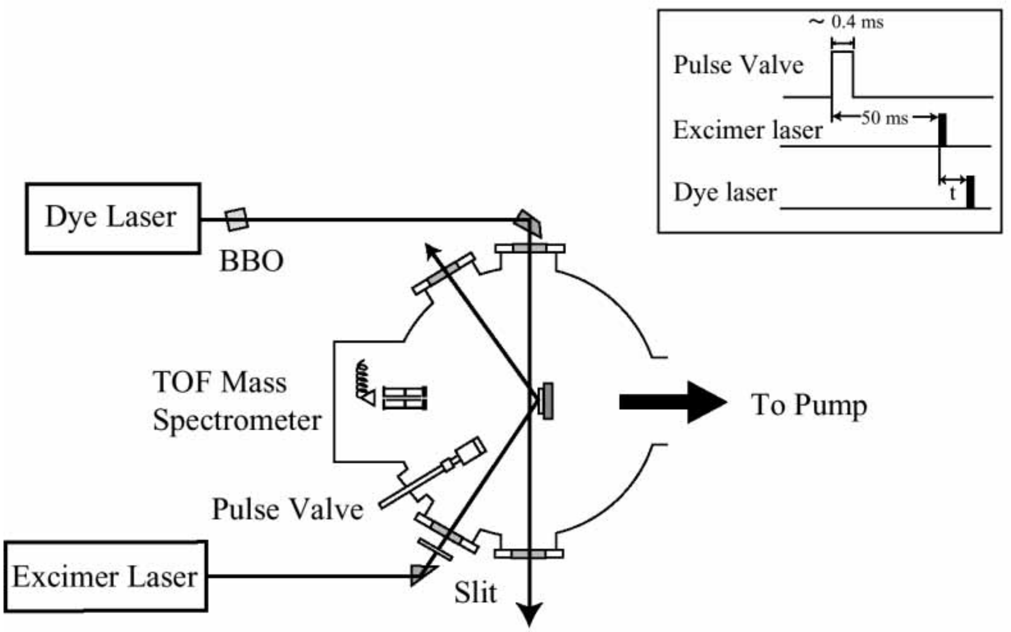

Figure 1. Experimental setup for TOF measurement. Flight time is defined as a function of delay time between dissociation and probe laser pulses. The inset shows the timing chart of pulsed beam of NO_2, dissociation laser pulse, and probe laser pulse.

2. Measurement of TOF Spectra of the Photofragment NO Molecules and O Atoms at Kyoto University. Experiments were performed in a vacuum chamber that is schematically shown in Figure 1. Its details have been described previously.[5] The base pressure of the chamber was 5×10^{-9} Torr. The TOF spectra of NO and O from the photodissociation of N_2O_4 on the ice film were measured by REMPI. An excimer laser (Lambda Physik, model COMPex, 10 Hz) was used for photodissociation. The output intensities were reduced on the ice surface to $I_{\text{laser}} < 1.5$ mJ cm^{-2} at 193 nm, $I_{\text{laser}} < 1.5$ mJ cm^{-2} at 248 nm, and $I_{\text{laser}} < 3.5$ mJ cm^{-2} at 351 nm. An Nd^{3+}–YAG laser-pumped dye laser was used as a probe laser (Lambda Physik, model SCANmate, 0.1 mJ/pulse at UV). The one-photon transition of NO($A^2\Sigma - X\ ^2\Pi_{3/2}$, $v'' = 0$, J'') was monitored by two-photon REMPI at 226 nm. O(^3P_j, $j = 0, 1, 2$) atoms were probed by the REMPI transition of O($^3D_{j'} - {}^3P_{j''}$) at 225.7–226.2 nm. The TOF spectra of NO and O were taken as a function of time delay, *t*, between the photolysis and probe laser pulses. A distance, *d*, from the ice surface to the detection region was variable for 3–5 mm and set to 3 mm for most of the experiments.

2.1. Deposition of NO_2 on Ice Films. For deposition of NO_2 gas onto the ice film, two different methods were used, the direct pulsed effusive beam method and the indirect backfilling method. We found no pronounced effect on the TOF spectra by changing the exposure methods. Therefore, the results with the direct deposition method are reported in this paper unless otherwise noted. NO_2 gas was prepared from a mixture of NO (300 Torr) with O_2 (610 Torr), which was deposited on a water–ice film by expanding the gas with a pulsed molecular beam head (General Valve) every 100 ms. Oxygen does not deposit on the ice film at 80–140 K. A stagnation pressure of the gas valve was 100 Torr of the gas mixture.

2.2. Preparation of Water–Ice Films. We used two different methods for the preparation of water–ice films in the TOF experiment, the collimated effusive H_2O beam method (direct deposition) and background deposition method (backfilling).[5] Amorphous solid-water (ASW) films were prepared by direct deposition of water on the polycrystalline Au substrate, with (111) domains at 85 K and a pulsed gas beam at the angle of incidence of 45°. The stagnation pressure of the gas beam was 20 Torr of neat water vapor. We prepared PASW films by backfilling at 90 K for 60 min on the Au substrate, which is characterized by a high porosity, a high surface area, and a low density.[25–27] Sato et al. estimated that the exposure of H_2O necessary to obtain 1 monolayer (ML) of ice film on an Au(111) substrate was 3 L at 90 K.[19] In the present experiment, the exposure was 1800 L, which resulted in formation of 600 ML of H_2O on Au for backfilling and more than 90 ML for direct deposition by the beam method. A PCI film was prepared by annealing the ASW film at $T = 130$ K for >5 min or the PASW film for 25 min and then cooling to an appropriate temperature.

Results

1. IRAS Measurement. 1.1. Interaction of N_2O_4 with Ice Surface. Figure 2 shows IRA spectrum of amorphous ice adsorbed on Au(111) at 93 K. The IRA bands of a thin ice film have been assigned previously.[15,28] The sharp band at 3700 cm^{-1} is assigned to the stretching mode of the free OH group at the ice surface, the broad and strong band at 3389 cm^{-1} to the OH stretching mode of bulk ice, and the weak band at 1654 cm^{-1} to the HOH bending mode of bulk ice. The IRA spectrum resembles the IR transmission spectrum of a water film at room temperature except for the 3700 cm^{-1} band,[29] indicating that the ice film on Au(111) is an amorphous ice layer.

The interaction of the free OH groups of amorphous ice surfaces with adsorbed N_2O_4 was examined by IRAS. The inset of Figure 2 shows intensity differences in IRA spectra before and after N_2O_4 adsorption at each temperature. Positive (upward) bands represent intensity reduction compared to the pure ice film case. The free OH band at 3700 cm^{-1} disappeared completely upon N_2O_4 adsorption at 100–115 K because all free OH groups interact with N_2O_4. In addition, the wide positive band centered at 3480 cm^{-1} indicates that the bulk OH groups also interact with N_2O_4 at $T = 100$–115 K. The fact that the center frequency of the bulk OH band is higher than the peak frequency of the pure amorphous bulk ice band by ~100 cm^{-1} suggests that N_2O_4 interacts also with the bulk OH group. For the crystalline ice surface, the interaction of the bulk OH group was also observed.

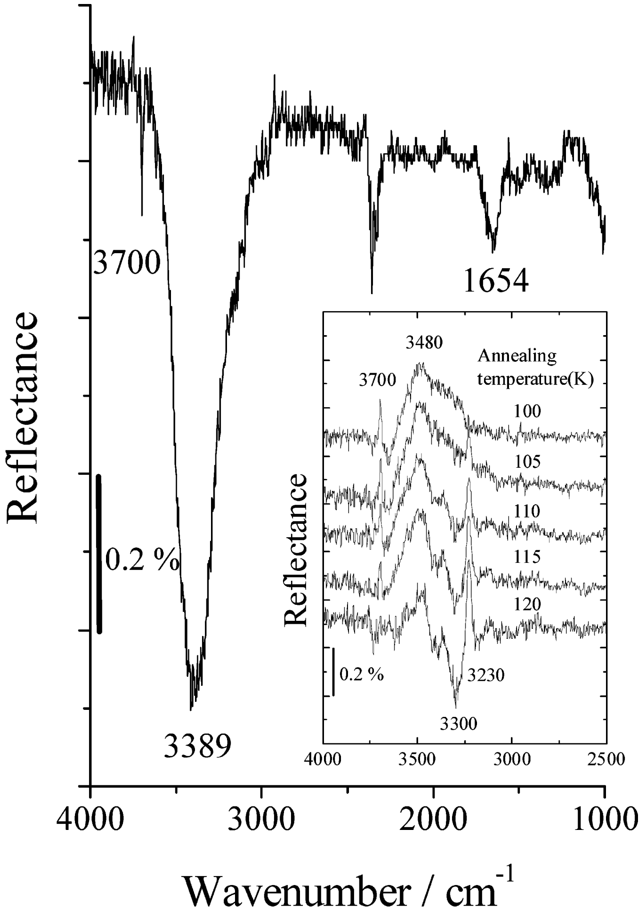

Figure 2. Infrared reflection absorption spectra of H_2O adsorbed on an Au(111) surface at 93 K for 4 L exposure. The inset shows a difference spectrum in the OH stretching region upon NO_2 adsorption on amorphous ice at 100 K. The difference spectrum is referred to that taken for bare ice. The coverages of H_2O and N_2O_4 are 5 and 1.5 ML, respectively.

1.2. Surface-Adsorbed Species on Ice Films. The NO_2 exposure necessary for one-monolayer coverage of NO_2 at 80−90 K was 4 L for a PCI film,16 L for an ASW film, and 2 L for an Au(111) substrate.[30] The IRA spectra of N_2O_4 (5 ML on PCI and 3 ML on ASW) are shown in Figure 3 and resemble those of N_2O_4 adsorbed directly on Au(111), except for the absence of the chemisorbed NO_2 band on Au at 1182 cm^{-1}.[23,31] The two bands at ~1300 cm^{-1} are attributed to the ONO symmetric stretching and the three bands at ~1750 cm^{-1} to the ONO asymmetric stretching of N_2O_4 with D_{2h} symmetry. The complete absence of the strong asymmetric stretching band of NO_2 at 1600−1650 cm^{-1} indicates the absence of NO_2 monomer, other NO_x compounds, and HONO. N_2O_4 isomers such as D isomers, $O{=}N{-}O{-}NO_2$, and nitrosonium nitrate, $NO^+NO_3^-$, were not detected in our IRA spectra. Although various kinds of NO_2 species are formed in a low-temperature inert gas matrix[32] and on substrates,[33−37] NO_2 adsorption on ASW and PCI films below 130 K results in formation of *pure* N_2O_4 (D_{2h}) layers. In addition, after adsorption of N_2O_4 on crystalline and amorphous ice at $T < 100$ K, the substrate temperature was elevated up to 230 K. Our results show that neither $NO^+NO_3^-$ nor D isomers were present. The assignment of IRAS bands was reported by Rieley et al. for the ordered monolayers of N_2O_4 by adsorption of NO_2 on an ice film of about 30 ML held on a Cu(100) substrate at 100 K.[15]

1.3. Molecular Orientation on Surface. IRAS is selectively sensitive to a vibrational mode perpendicular to a reflective metal surface due to surface selection rules; hence, we can obtain information about molecular orientation with respect to a surface.[38] When the IRA spectrum of the first-layer N_2O_4 on crystalline ice was measured, the 1300 cm^{-1} band of ONO symmetric stretching has an intensity comparable to the 1750 cm^{-1} band of ONO asymmetric stretching.[15] Since an IR transmission spectrum of gas-phase N_2O_4 exhibits both the symmetric and asymmetric ONO stretching bands in comparable intensities, the first-layer N_2O_4 on crystalline ice should be randomly oriented. About the multilayered N_2O_4 on PCI, N_2O_4 forms tightly packed ordered layers with the N−N axes canted at 10° to the surface normal.[16,17]

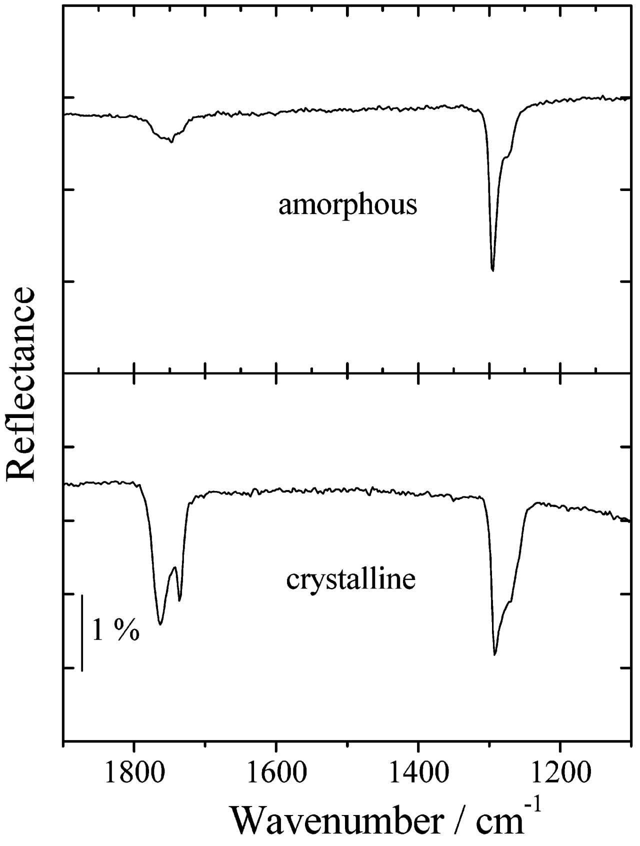

Figure 3. Infrared reflection absorption spectra of N_2O_4 on amorphous and crystalline ice films at $T = 120$ K. The ONO symmetric band appears at 1303 cm^{-1} and the asymmetric stretching band at 1750 cm^{-1}. The coverage of N_2O_4 is 5 ML on polycrystalline ice and 3 ML on amorphous solid water.

2. TOF Spectra and Rotational Spectra of NO($v = 0, J$) Photofragments from N_2O_4 Adsorbed on Water−Ice Films.

2.1. Preparation of N_2O_4 Layers on Ice Films with the Intermittent Exposure. The pulsed molecular beam of the mixture gas of NO_2 and O_2 was directed to the surface of the ice film with an intermittent exposure scheme. The delay between the molecular beam and the photolysis laser trigger was typically set to 50 ms, as shown in the inset of Figure 1. For the amorphous ice film at $T = 80$ K and 193 nm, the signal intensity of the product NO increased linearly up to $P = 10 \times 10^{-8}$ Torr, where P stands for the total pressure of the vacuum chamber. Thus, we assume that a coverage of 1 ML for N_2O_4 on ASW at 80 K was achieved at $P = 10 \times 10^{-8}$ Torr. In our previous experiment with the pulsed molecular beam of the same gas mixture, the intermittent exposure of NO_2 on a cooled polycrystalline Au(111) substrate $T = 80$ K formed one ML N_2O_4 for $P = 1 \times 10^{-8}$ Torr.[22] The pressure ratio (10×10^{-8}/

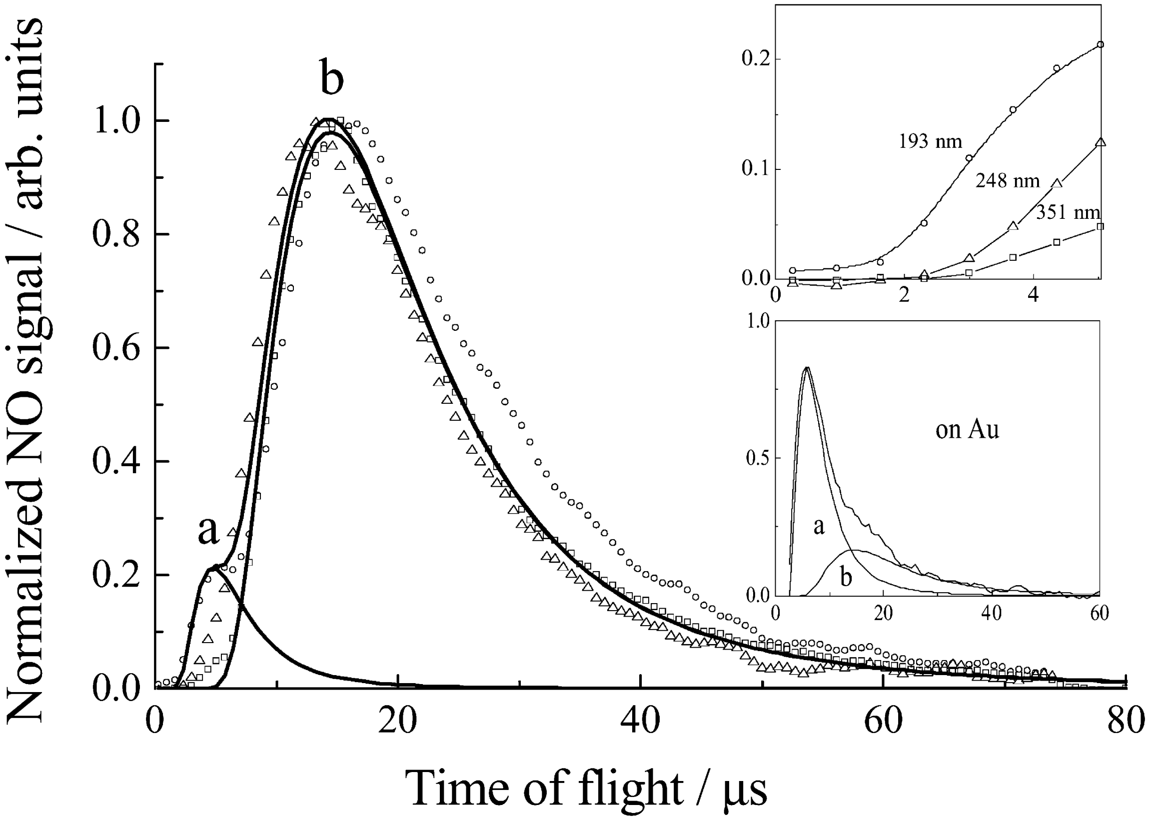

Figure 4. TOF spectra of NO($X^2\Pi_{3/2}$, $v = 0$, Q-head) from the photodissociation of N_2O_4 on an amorphous ice film at dissociation laser wavelengths, 193 nm (○), 248 nm (△), and 351 nm (□). Ice temperature $T = 80$ K and chamber pressure $P = 10 \times 10^{-8}$ Torr. (N_2O_4 coverage of 1.2 ML.) The smooth solid curve is a Maxwell−Boltzmann energy distribution defined in eq 1 with translational temperature $T_{\text{trans}} = 100 \pm 15$ K. The upper inset shows the enlarged spectra at the threshold region. The lower inset shows a typical spectrum of NO($v = 0$) from the 193 nm photodissociation of N_2O_4 adsorbed directly on Au at 85 K, which consists of two components (a) $T_{\text{trans}} = 600 \pm 30$ K and (b) $T_{\text{trans}} = 80 \pm 10$ K.

1×10^{-8}) is 10 for the ASW/Au substrates. These results are indistinguishable from the literature value of 8; that is, the NO_2 exposure necessary for one ML coverage of NO_2 at 80−90 K was 16 L for an ASW film and 2 L for an Au(111) substrate.[30] As the substrate temperature increases above 90 K, the coverage decreases due to lowering of the sticking probability.

2.2. Measurement of TOF Spectra and Rotational Spectra. TOF spectra of NO($v = 0$, Q-head) from the photodissociation of N_2O_4 on ASW and PCI films at 193, 248, and 351 nm were measured for various NO_2 pressures ($P = 1{-}10 \times 10^{-8}$ Torr) and $T = 80{-}120$ K. Vibrationally excited NO($v \geq 1$) was not observed. The TOF distributions were almost independent of the morphology of the ice surfaces. Typical TOF spectra of NO are shown in Figure 4 for $P = 10 \times 10^{-8}$ Torr on ASW at $T = 80$ K. This pressure condition for NO_2 corresponds to a N_2O_4 monolayer. A very slow TOF component ($T_{\text{trans}} = 11 \pm 3$ K) with a small contribution appeared after $t = 30$ μs. This component is considered to be an artifact caused by the NO photofragments that were scattered once and bounced back to the REMPI detection region.[17,22] This slowest component was subtracted from the TOF spectra in the following analysis.

2.3. Translational Temperatures of NO($v = 0$) Photofragments. To simulate the TOF spectra, a flux-weighted Maxwell−Boltzmann (MB) distribution and a Gaussian distribution were used. We found that a composite of two MB distributions with translational temperatures, T_{trans}, fit well to the observed TOF distributions. Conversion from the energy distribution to the TOF distribution was performed using the reported Jacobian.[39] The TOF spectrum $S(t)$ of Figure 4 is fitted by a composite of two flux weighted MB distributions, $P_{\text{MB}}(E_t)$, and a coefficient, a. This energy distribution is characterized by the average energy $\langle E_t \rangle = 2k_BT_{\text{trans}}$[39]

$$S(a,t,T_1,T_2) = aS_{\text{MB}}(t,T_1) + (1 - a)S_{\text{MB}}(t,T_2) \qquad (1)$$

$$S_{\text{MB}}(t,r) = r^3t^{-4}\exp(-mr^2/(2k_BT_{\text{trans}}t^2)) \qquad (2)$$

$$P_{\text{MB}}(E_t) = (k_BT_{\text{trans}})^{-2}E_t\exp(-E_t/(k_BT_{\text{trans}})) \qquad (3)$$

where r is a flight length for photofragment and k_B is the Boltzmann constant. The TOF distributions consist of a fast component and a slow component. For the angular distribution of the photofragments from the ice surface, $\cos^n\theta$, where θ is the surface polar coordinate, $n = 0$ was adopted in the best-fitting procedures because the parent molecules N_2O_4 adsorb randomly on the PCI and ASW surfaces as described above. For the fast component of the 193 nm result, T_{trans} are 950 ± 150 K. Only a small change was observed in the translational temperatures for the three different dissociation laser wavelengths, which is within our experimental error bars. The TOF distributions consist of a fast component (a) $T_{\text{trans}} = 950 \pm 150$ K and a slow component (b) 100 ± 15 K for both amorphous and crystalline ice films. The contribution of the slow component becomes slightly larger at the longer wavelength, 93 ± 7% for 193 nm, 97 ± 3% for 248 nm, and 99 ± 1% for 351 nm.

Susa and Koda reported that the TOF distribution of the NO photofragments is bimodal, fast (1700 ± 350 K) and slow (100 ± 10 K), and their relative intensities are 1−0.86 for non-annealed ice and 1−0.22 for annealed ice.[18] The reason for the discrepancy between our and their translational temperatures is

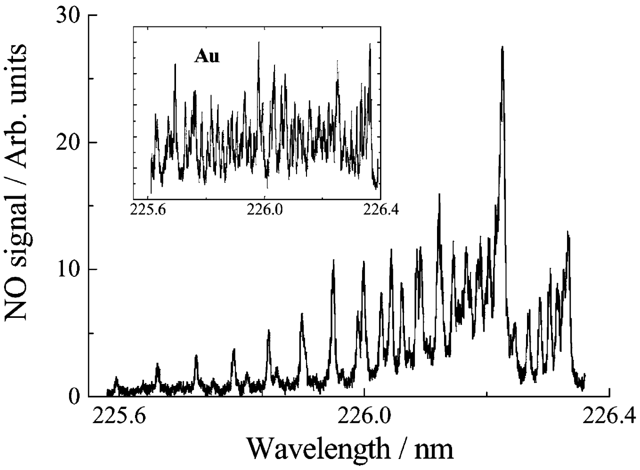

Figure 5. A rotational spectrum of the O−O band of NO(A−X) from the photodissociation of N_2O_4 on amorphous ice at 193 nm. TOF = 5 μs, ice temperature $T = 85$ K, and chamber pressure $P = 5 \times 10^{-8}$ Torr. (0.6 ML of N_2O_4.) The inset shows a corresponding spectrum from the photodissociation of N_2O_4 on Au.

not clear, but their laser intensity was 5 mJ cm^{-2} for a 20-ns pulse, 10 times stronger than our laser intensity, and they reported that the initial stage of dissociation was due to multilayered N_2O_4 and not N_2O_4 directly interacting with an ice surface. A fast-component temperature of 1000 K was also reported in their paper. We believe that the discrepancy in the translational temperature of the fast component and its relative contribution to the total TOF signal intensity comes from the difference in the degree of interaction of N_2O_4 with the ice surface.

The threshold TOFs of the fast components, t_0, become faster as the photon energy is increased from 248 to 193 nm (the upper inset of Figure 4) because these threshold TOFs reflect directly the reaction excess energies. For 193 nm, the threshold TOF, t_0, is 1.0 ± 0.3 μs, and for 248 nm, $t_0 = 2.0 \pm 0.5$ μs. For 351 nm, t_0 is not clearly seen but is about 3 μs.

For comparison purposes, the lower inset of Figure 4 shows a typical TOF spectrum of NO($v = 0$) from the 193-nm photodissociation of N_2O_4 adsorbed directly on the polycrystalline Au substrate. The TOF spectrum consists of a fast component (a) with $T_{trans} = 600 \pm 30$ K and a slow one (b) with $T_{trans} = 80 \pm 10$ K.[22] The fast component (a) is dominant in the TOF spectrum for the Au experiment, while the slow one (b) is dominant in the present ice experiment. In addition, the vibrationally excited NO($v = 3$) was produced in the Au experiment at 193 and 248 nm, while vibrationally excited states NO($v \geq 1$) are not produced in the present ice experiment.

2.4. Rotational Spectra. Figure 5 shows a typical rotational spectrum of NO($A^2\Sigma$, $v' = 0$, J' − $X^2\Pi_{3/2}$, $v'' = 0$, J'') from the 193 nm photodissociation of N_2O_4 on amorphous ice at $T = 80$ K. This spectrum was measured at $t = 13$ μs. The estimated rotational temperature is $T_{rot} = 175 \pm 25$ K. At 248 and 351 nm the results are essentially the same. For comparison purposes, a typical rotational spectrum of NO from N_2O_4 on Au at 193 nm is shown in the inset of Figure 5. The NO fragment is highly rotationally excited.

2.5. Incident Laser Power Dependence. Figure 6 shows the photolysis laser power dependence on the NO signal intensity of the slow component from the photodissociation of N_2O_4 on PCI at 193 and 248 nm. Up to 1 mJ cm^{-2} the slope is unity, suggesting a one-photon process for NO production. The power dependence of signal intensity at 351 nm was also unity.

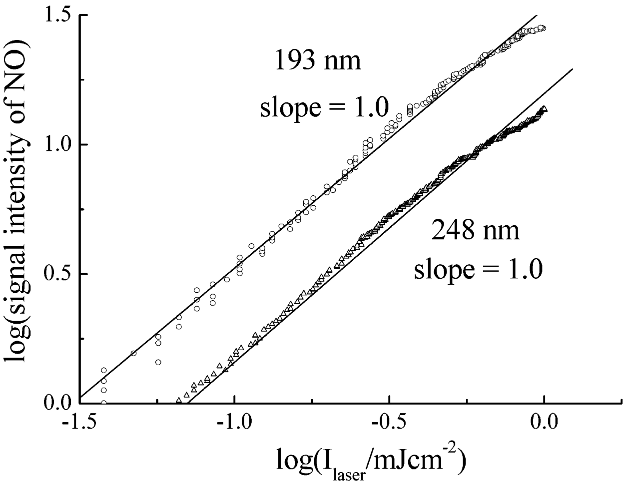

Figure 6. Photolysis laser power dependence on the NO($v = 0$, Q-head) slow-component signal intensities for 193 nm (○) and 248 nm (△).

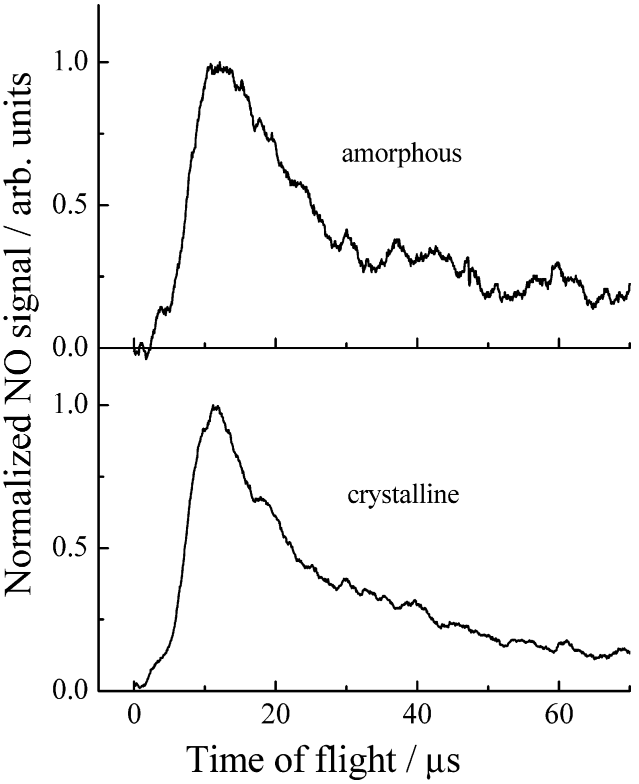

Figure 7. TOF spectra of NO($v = 0$, Q-head) from the 193-nm photodissociation of N_2O_4 adsorbed on amorphous and crystalline ice films for ice film temperature $T = 120$ K and chamber pressure $P = 10 \times 10^{-8}$ Torr. (N_2O_4 coverage of 1.2 ML.)

2.6. Effect of Adsorbed States of N_2O_4 on TOF Spectra at 193 nm. Figure 7 shows TOF spectra of NO from N_2O_4 on amorphous and crystalline ice films at $T = 120$ K and $P = 10 \times 10^{-8}$ Torr. At this temperature and pressure, the thickness of the N_2O_4 layer on amorphous and crystalline ice is estimated to be 0.6 and 2.5 ML, respectively. There is no noticeable difference between the two TOF spectra. Although the annealing process from 91 to 120 K converts the disordered N_2O_4 to the ordered N_2O_4 on the crystalline ice film, this change has no effect on the relaxation dynamics of the photofragments. However, as will be described in the following section, there is a large difference in the absolute signal intensities between amorphous and crystalline ice films.

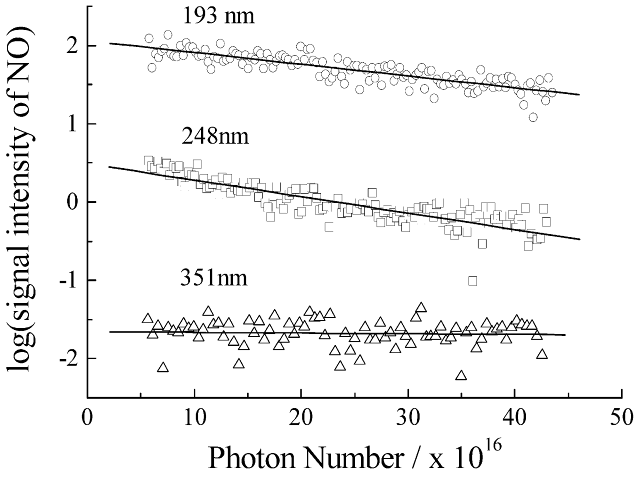

Figure 8. Signal decay curves of the NO($\upsilon = 0$, Q-head) slow component as a function of total photon numbers irradiated on N_2O_4 at 193, 248, and 351 nm. 1 ML of N_2O_4 on the amorphous ice film at 80 K.

2.7. Photodissociation Cross Section. The decay curves of the NO signal intensity were measured as a function of irradiation time after the sample molecules were once exposed on PCI at 90 K under 1 ML condition. Since the photodissociation process follows a simple exponential law, eq 4 determines the photodissociation cross section of N_2O_4, σ_{diss}, or the absorption cross section σ_{abs} multiplied by dissociation quantum yield ϕ

$$N = N_0 \exp(-\sigma_{\text{diss}} n_{h\nu}) \tag{4}$$

where N is the residual amount of the sample molecules on the PCI surface, N_0 the initial amount of the sample molecules, and $n_{h\nu}$ the number of photons.[40] The results are shown in Figure 8, from which we derive $\sigma_{\text{diss}} = (2 \pm 1) \times 10^{-18}$, $(3 \pm 1) \times 10^{-18}$, and $(0.1 \pm 0.1) \times 10^{-18}$ cm^2 at 193, 248, and 351 nm, respectively. Hasselbrink et al. reported σ_{diss} (193 nm) $= 3 \times 10^{-18}$ cm^2 for the NO formation from N_2O_4 adsorbed on top of a NO-saturated Pd surface.[20] Susa and Koda reported that the cross section at 193 nm was (10−60) $\times 10^{-18}$ cm^2, which is approximately 20−100% of the gas-phase photoabsorption cross section σ_{abs} of N_2O_4, i.e., 52.8×10^{-18} cm^2.[41] Our cross sections on PCI are much smaller than those reported by Susa and Koda. The reason for the discrepancy between their data and ours, we suspect, is that in our case the photodissociation quantum yield ϕ becomes small, e.g., dissociation is efficiently quenched by the interaction with the grain boundaries of the PCI surface. Actually, in the case of ASW by Susa and Koda, the desorption cross section of NO_2 and NO at 193 nm was (0.36−8.3) $\times 10^{-18}$.[18] Sato et al. reported that the dissociation cross sections of the N_2O_4 multilayers on Au(111) are 2.8×10^{-18} and 0.56×10^{-18} cm^2 at 260 and 350 nm, respectively,[23] which are close to the absorption cross sections in the gas phase.

3. REMPI Detection of NO Photofragments by TPPS. Photodesorbed NO signal intensities for $P = 1.5 \times 10^{-8}$ Torr or 1.5 ML of N_2O_4 on polycrystalline Au, 0.8 ML on PCI and 0.2 ML on ASW were measured as a function of the substrate temperature T. We refer to this measurement as REMPI-TPPS, in which NO is probed by the REMPI method with increasing T at a rate of 2 K s^{-1}. Note that this TPD is different from an ordinary TPD in that the ice surface was exposed to an NO_2 molecular beam between the photodissociation laser shots. Figure 9 shows the REMPI-TPPS spectra of NO from the 193-nm photodissociation of N_2O_4 on ASW and PCI. For ASW, a monotonic decrease of the signal intensity was observed with increasing T. Since our IRAS measurement indicates that the phase change of ASW to PCI occurs at $T > 120$ K,[19] the signal intensity is not associated with the free OH concentration on the amorphous ice surface. The signal intensity is directly related to the sticking probability of NO_2 on water−ice films, which decreases with substrate temperature.

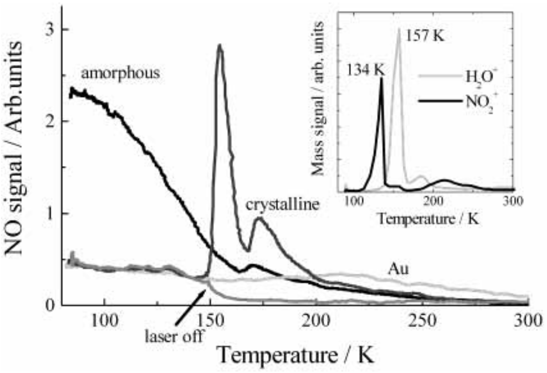

Figure 9. The signal intensities of NO($\upsilon = 0$, Q-head) from N_2O_4 on amorphous and crystalline ice films for temperature-programmed photodetachment spectroscopy. $P = 1.5 \times 10^{-8}$ Torr, $\lambda = 193$ nm, and $I_{\text{laser}} = 1.5$ mJ cm^{-2} pulse^{-1}. The substrate temperature increases at a rate of 2 K s^{-1}. The curves of the inset show a conventional temperature-programmed desorption spectrum of NO_2 and H_2O from N_2O_4 (1.6 ML) on an ice film without photoirradiation, using a mass spectrometer (taken from ref 19). The arrow (laser off) shows the position at which the laser light was shut off for the crystalline film. See text for details.

Figure 9 also shows a spectrum for 1.5 ML on Au. The REMPI-TPPS profiles of NO are similar to those on PCI in the temperature range $T = 80-150$ K. At $T > 150$ K, however, these two REMPI-TPPS spectra are different. For PCI, the spectrum is characterized by two peaks of NO at 155 and 173 K. These peaks correspond to those of H_2O at 157 and 187 K. Shown in the inset is a conventional TPD spectrum of N_2O_4 (1.6 ML) on an ice film, in which the 157 K peak is assigned to H_2O desorption and the 187 K peak corresponds to the adduct formation of H_2O with NO_2.[19] Thus, N_2O_4 is retained in the grain boundaries of the polycrystalline ice films. In our REMPI-TPPS the N_2O_4 retained in the grain boundaries become free at the water−ice sublimation temperature, and hence the apparent dissociation quantum yield increases, that is, the NO signal intensity increases. Another plausible explanation for this signal intensity enhancement is the following. Since water−ice films are transparent at 193 nm, (a) NO may be photoproduced and trapped by the photodissociation of N_2O_4 in the ice grain boundaries during the irradiation at 193 nm before the substrate temperature increased up to 155 K and (b) NO thus produced and trapped in the grain boundaries were released into the gas phase upon melting the ice film at 157 K. To check if this process could have caused the 157 K peak of NO, the 193-nm irradiation was kept continuous from $T = 80$ to 150 K and then was turned off at $T > 150$ K as marked by the arrow in Figure 9. In this case, the 157 K peak was not detected. These results suggest that even if N_2O_4 trapped in a grain boundary is irradiated at 193 nm, NO is not trapped in the ice film.

4. Resonance-Enhanced Multiphoton Ionization (REMPI) Detection of O(^3P_j) Atoms. Two-photon REMPI signals of O(^3P_j) atoms from N_2O_4 photodissociation at 193 and 248 nm were found, while not at 351 nm. The O(^3P_j) atom is mostly populated in the lowest level, $j = 2$. The observed TOF and excitation spectra for O(^3P_j) are shown in Figure 10 for 193 nm. The translational temperatures of the fast and slow

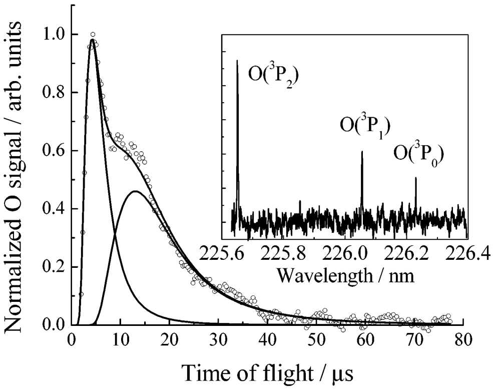

Figure 10. REMPI-TOF spectra of $O(^3P_2)$ from the photodissociation of N_2O_4 adsorbed on an amorphous solid water−ice film at 193 nm. The smooth solid curves are Maxwell−Boltzmann energy distributions defined in eq 1. The insets show the REMPI excitation spectra of $O(^3P_j)$. Substrate temperature $T = 80$ K and chamber pressure $P = 10 \times 10^{-8}$ Torr. (N_2O_4 coverage of 1.2 ML.)

components are 1050 ± 150 and 100 ± 10 K. As a reference experiment, we previously performed detection of $O(^3P_j)$ atoms from N_2O_4 adsorbed directly on Au at 193 nm. The probed $O(^3P_j)$ atoms are much more populated up to the highest level, $j = 0$.[22] Sato et al. speculated that for N_2O_4 on a thin PCI prepared on an Au substrate a part of the oxygen atoms reach the Au substrate and appear as surface oxygen molecules in their TPD spectra.[23]

Discussion

1. Primary Processes of N_2O_4 Photodissociation on Ice Films. 1.1. Photodissociation at 193 and 248 nm. The IRAS measurement shows no presence of NO_3 or N_2O_3 on the Au surface during the irradiation at 260−420 nm.[23] $O(^3P)$ atoms are detected by REMPI at 193 and 248 nm and not at 351 nm. The linear increase of the NO signal intensity as a function of the dissociation laser power suggests a one-photon dissociation. In addition, the threshold TOFs are shorter for the shorter dissociation wavelengths. The observed absorption cross sections are reasonably large. Susa and Koda measured the relative yield of the products with mass spectrometric methods, $NO_2/NO/O_2 = 1.0/1.1/0.01$ for PCI.[18] Hence, the major dissociation channel at 193 and 248 nm is process (I)

	ΔH (kJ mol^{-1})	$\lambda_{\mathrm{threshold}}$ (nm)	
$N_2O_4 \rightarrow NO_2 + NO + O$	368	325	(I)
$NO_3 + NO$	278	430	(II)
$N_2O_3 + O$	322	370	(III)
$NO_2 + NO_2$	175	682	(IV)

The reaction enthalpies are calculated from the gas-phase thermodynamic values. The photon energies at 193 and 248 nm are above the threshold energy of reaction III. Susa and Koda claimed that the experimentally observed kinetic energies of the fast photofragments at 193 nm can be explained by the statistical prediction of the reaction available energy if the dissociation is to produce $NO_2(X) + NO_2\ (2^2B_2)$, one of which then predissociates to produce NO + O.[18] Essentially the same interpretation was applied to the dissociation dynamics of N_2O_4 in the gas phase.[42] This mechanism can explain the fact that the translational energies are almost the same in photodissociation processes at both 193 and 248 nm and the slow component is dominant. The NO and O fragments are translationally and internally relaxed, while those fragments from the Au substrate are highly excited. These results suggest that the water−ice films, PCI, and ASW work as an efficient thermal bath to the randomly oriented N_2O_4 monolayer on them.

1.2. Photodissociation at 351 nm. The photon energy of 351 nm is below the gas-phase dissociation threshold of 325 nm for reaction I by 28 kJ mol^{-1}. The formation of NO from N_2O_4 on metal surfaces at 351 nm, which is attributed to the electron-mediated process, was reported by Hasselbrink et al.[20] and Sato et al.[23] In their experiment, a falloff of the signal intensity was observed for the high coverage region. Their results indicate that the photoproducts released by the irradiation at ∼350 nm are only from the layers near the N_2O_4−Au interface. Since electron transfer from a metal surface through the water layer is prohibited,[43] it is unlikely in the present experiment that the dissociation takes place via the surface-mediated processes. Rieley et al.[17] investigated the photodissociation of N_2O_4 multilayers on water layers (30 ML)/Cu at 355 nm. The direct photoabsorption process of N_2O_4 generates NO_2 due to N−N bond scission. No desorption of N_2O_4 occurred at this wavelength. In the present experiment, NO_2 desorption followed by its one-color dissociation process at the probe laser wavelength 226 nm may give an NO signal. However, we can eliminate this possibility because (a) $O(^3P_j)$ was not detected in our experiment, (b) the translational energy of NO is low, and (c) the threshold TOF at 351 nm is slower than those at 193 and 248 nm.

The difference in the desorption enthalpies may explain the energy deficit problem if we assume the following surface-involved reaction scheme, based on the fact that the formation of O atoms on the Au(111) surface was observed when N_2O_4 on PCI was photodissociated by a high-pressure Xe lamp at 240−400 nm[23] but not in the present gas-phase detection

$$N_2O_4(\mathrm{ad}) + 351\ \mathrm{nm} \rightarrow NO + O(\mathrm{ad}) + NO_2(\mathrm{ad}) \quad (\mathrm{V})$$

The desorption enthalpy of N_2O_4 on an ice surface is 39 kJ mol^{-1}.[15] If the sum of the desorption enthalpies of $O(^3P)$ atom and NO_2 is larger than (39 + 28) kJ mol^{-1}, we could explain our results. Unfortunately these data are not available. However, the fact that the relative yield of O_2 against NO at 193 nm are 1% for PCI and 10% for ASW suggests that the oxygen atoms are easily trapped by grain boundaries of ice.[18]

Process II to NO_3 + NO is another plausible process for the formation of NO at 351 nm. At 351 nm, however, the major primary photodissociation process in the gas phase is process IV to $2NO_2$. For N_2O_4 adsorbed directly on ice, a possible explanation for the formation of NO via reaction II at 351 nm is the change in the electronic structures of N_2O_4 upon adsorption on ice. If so, then, the photoabsorption cross sections should be changed. The gas-phase absorption cross sections σ_{abs} of N_2O_4 is 0.7×10^{-18} cm^2 at the first maximum (340 nm). At shorter wavelength, it increases up to 57×10^{-18} cm^2 at the third maximum (186 nm). In fact, our results, σ_{diss} at 193 and 351 nm, are smaller than those for the gas-phase N_2O_4 by an order of magnitude, but σ_{diss} at 248 nm is close to that of the gas phase. Since the value of ϕ on PCI is expected not to vary as a function of dissociation wavelength, the large difference between the gas-phase and the surface-phase cross sections suggests that the interaction of N_2O_4 with the ice surface changes the electronically excited potential surfaces. Thus, the primary process II becomes a plausible process on the surface. Because of the weak photoabsorption at 351 nm, neither NO_3 nor N_2O_5 were detected with our IRAS sensitivity.

Involvement of HNO_3 and HONO on the ice surface is unlikely because our IRAS measurement showed no presence of these species on the surface, although Wang and Koel reported that a small amount of these species were formed from the coadsorbed layers of NO_2 on H_2O below 145 K.[45] Only at room temperature is NO_2 on H_2O suspended in silica easily converted to these species.[46,47] Since our experimental temperature is 80−120 K, N_2O_4 is the only species involved in the 351 nm photolysis.

The following sequential two-photon process of the adsorbed species may be a possible primary process

	ΔH (kJ mol^{-1})	
$N_2O_4 \rightarrow NO_2(ad)$	175	(IV)
$NO_2(ad) \rightarrow NO + O$	$100 + x$	(VI)

where x stands for the desorption enthalpy of NO_2, which could be a few tens of kJ mol^{-1}. The excess energy for the 351-nm one-photon photolysis via process VI is $(240 - x)$ kJ mol^{-1}, which could be larger than 113 kJ mol^{-1} for process I at 248 nm. If process VI were dominant at 351 nm, the threshold TOF t_0 would be short and the O atom would be probed. Actually, t_0 from 351 nm was much longer than that for 248 nm, and no O atoms were detected. In addition, the power dependence at 351 nm was unity. Thus, this sequential two-photon process would not occur at 351 nm.

2. Adsorption of N_2O_4 on Water−Ice Films. The upper surface of an amorphous ice film is characterized by free OH groups. Graham and Roberts reported that the difference in adsorption probabilities of HCl on ASW and PCI films is attributed to a lower coverage of the free OH groups at the PCI surface.[48] Schaff and Roberts investigated the difference in surface chemical behavior between ASW and PCI.[49] Adsorption and desorption behaviors of polar and nonpolar molecules strongly depend on hydrogen donor ability of the ice surfaces. Porosity and surface area differences are not significant factors in the interaction of adsorbates with ice surfaces. They found two different desorption states of acetone on ASW, hydrogen-bonded and physisorbed ones.[50] Only the physisorbed one was observed on crystalline ice films. Their FT-IRAS measurements show that the free-OH coverage on the surface of PCI is approximately one-sixth of that on ASW.

As shown in the REMPI-TPPS spectra of Figure 9, the signal intensity on the crystalline ice is much weaker than on the amorphous ice. The substrate temperature dependence of the signal intensity for the amorphous ice may be explained by the decrease of the free OH group concentration on the surface. However, our IRAS measurements indicate the phase change of ASW to PCI occurs at $T > 120$ K.[19] Therefore, the decrease of the signal intensity at $T < 120$ K is not associated with the free OH concentration on the amorphous ice surface.

Stevenson et al. investigated the temperature dependence of the porosities of ASW, measuring N_2 adsorption by ASW. Above ~90 K, ASW films have essentially the same N_2 adsorption as the crystalline reference state at 145 K.[25] Thus porosity change cannot explain the present REMPI-TPPS results. Consequentially, the other possible explanation is considered, that is, the decrease of the sticking probability of N_2O_4 with substrate temperature. Sato et al. measured TPD spectra of NO after the ASW surface was exposed to NO_2 gas at each temperature $T = 90$, 100, 110, and 120 K.[30] The TPD intensity decreased as the ice temperature increased. Since the adsorbed amount of N_2O_4 is proportional to the TPD intensity, it is concluded that the change in sticking probabilities of NO_2 on the ice films caused these results.

The TPD peak of NO_2 in the inset of Figure 9 at 134 K is attributed to sublimation of physisorbed N_2O_4 on the ice film. At 214 K, another TPD peak of NO_2 appears. The 214-K peak comes from the fact that a part of the N_2O_4 adsorbed on the ice film is held in the bulk phase of ice and then moves onto the Au surface upon heating. The TPD of H_2O exhibits two peaks at 157 and 185 K. The 157 K peak is identical to that from pure H_2O/Au(111), while the 185 K peak is due to the adduct formation of H_2O with NO_2. When the thickness of PCI was less than 4 ML, the band ascribed to the NO_2 chemisorbed directly on Au was observed in IRAS, indicating that NO_2 or N_2O_4 can reach the Au surface through grain boundaries of PCI.[19] Sadtchenko et al. also reported the trapping of HCl in the grain boundaries of PCI.[51] In the present experiment, the ice film was so thick that N_2O_4 was retained only in bulk ice. Thus, REMPI-TPPS spectra on the ice films showed no peak at 214 K, while there is a wide peak at 214 K in the TPD spectrum on the Au.

Susa and Koda reported that the relative yield of NO_2 from N_2O_4 on ASW at 193 nm is 10 times smaller than NO.[18] They interpreted that the once-photoproduced NO_2 in the ASW ice is likely to be readsorbed in the porous ice while NO adsorption does not occur at 80 K. Thus, N_2O_4 is retained either in the grain boundaries of the polycrystalline ice film and in micropores of the amorphous ice films. The abrupt increase of the NO signal in our REMPI-TPPS clearly shows this trapped N_2O_4.

Conclusion

When NO_2 is deposited on amorphous and crystalline water−ice films at 80−140 K, N_2O_4 is the solo surface species on ice. N_2O_4 are also retained either in the grain boundaries of the polycrystalline ice film and in micropores of the amorphous ice films. The randomly oriented monolayer of N_2O_4 on the ice surface is photodissociated to produce NO. At 193 and 248 nm, the primary process is $NO + O + NO_2$. At 351 nm, other plausible primary processes are $NO + NO_3$. The TOF distribution of NO($v = 0$) consists of the major slow component with the translational temperature of 100 ± 15 K and the minor fast component with $T_{trans} = 950 \pm 150$ K for both amorphous and crystalline ice films. The translational and internal energy distributions of the NO molecules and O atoms are mostly relaxed because the ice surface works as an efficient bath for energy transfer, which are almost accommodated to the ice temperature. The contributions of the accommodated component in the signal intensity are 93 ± 7% for 193 nm, 97 ± 3% for 248 nm, and 99 ± 1% for 351 nm. There is no appreciable difference in the energy distributions of the photodissociation products at the three different dissociation wavelengths and also for the two different ice states, amorphous and crystalline.

The dissociation cross sections of N_2O_4 on ice films are $\sigma_{diss} = (2 \pm 1) \times 10^{-18}$, $(3 \pm 1) \times 10^{-18}$, and $(0.1 \pm 0.1) \times 10^{-18}$ cm^2 at 193, 248, and 351 nm, respectively, which are smaller than the gas-phase photoabsorption cross sections at the corresponding wavelengths, suggesting the small photodissociation quantum yield and also a change in the potential curves of N_2O_4 due to the interaction with the water−ice surface.

Acknowledgment. This work is supported by a grant-in-aid for the priority field "Radical Chain Reactions" from the Ministry of Education, Japan.

References and Notes

(1) Honrath, R. E.; Peterson, M. C.; Guo, S.; Dibb, J. E.; Shepson, P. B., Campbell, B. *Geophys. Res. Lett.* **1999**, *26*, 695.

(2) Dubowski, Y.; Colussi, A. J.; Hoffmann, M. R. *J. Phys. Chem. A* **2001**, *105*, 4928.

(3) Dubowski, Y.; Colussi, A. J.; Boxe, C.; Hoffmann, M. R. *J. Phys. Chem. A* **2002**, *106*, 6967.
(4) Moore, M. H.; Hudson, R. L.; Gerakines, P. A. *Spectrochim. Acta* **2001**, *A57*, 843.
(5) Yabushita, A.; Inoue, Y.; Senga, T.; Kawasaki, M.; Sato, S. *J. Phys. Chem. B* **2002**, 106, 3151
(6) Watanabe, A.; Kouchi, A. *Astrophys. J.* **2002**, *567*, 651.
(7) Pursell, C. J.; Conyers, J.; Denison, C. *J. Phys. Chem.* **1996**, *100*, 15450.
(8) Graham, J. D.; Roberts, J. T.; Brown, L. A.; Vaida, V. J. *J. Phys. Chem.* **1996**, *100*, 3115.
(9) Gane, M. P.; Williams, N. A.; Sodeau, J. R. *J. Chem. Soc., Faraday Trans.* **1997**, *93*, 2747.
(10) Gerakines, P. A.; Moore, M. H.; Hudson, R. L. *Astron. Astrophys.* **2000**, *357*, 793.
(11) Nishi, N.; Shinohara, H.; Okuyama, T. *J. Chem. Phys.* **1984**, *80*, 3898.
(12) Ogasawara, H.; Kawai, M. *Surf. Sci.* **2002**, *502*−*503*, 285.
(13) Yabushita, A.; Kawasaki, M.; Sato, S. *J. Phys. Chem. B* **2003**, *107*, 1472.
(14) Chaabouni, H.; Schriver-Mazzuoli, L.; Schriver, A. *Low Temp. Phys.* **2000**, *26*, 712.
(15) Rieley, H.; McMurray, D. P.; Haq, S. *J. Chem. Soc., Faraday Trans.* **1996**, *92*, 933.
(16) Rieley, H.; Colby, D. J.; McMurray, D. P.; Reeman, S. M. *Surf. Sci.* **1997**, *390*, 243.
(17) Rieley, H.; Colby, D. J.; McMurray, D. P.; Reeman, S. M. *J. Phys. Chem. B* **1997**, *101*, 4982.
(18) Susa, A.; Koda, S. *J. Atom. Chem.* **2003**, *43*, 197.
(19) Sato, S.; Yamaguchi, D.; Nakagawa, K.; Inoue, Y.; Yabushita, A.; Kawasaki, M. *Langumuir* **2000**, *16*, 9533.
(20) Hasselbrink, E.; Jakubith, S.; Nettesheim, S.; Wolf, M.; Cassuto, A.; Ertl, G. *J. Chem. Phys.* **1990**, *92*, 3154.
(21) Dixon-Warren, St. J.; Jackson, R. C.; Polanyi, J. C.; Rieley, H.; Shapter, J. G.; Weiss, H. *J. Phys. Chem.* **1992**, *96*, 10983.
(22) Senga, T.; Yabushita, A.; Inoue, Y.; Kawasaki, M.; Sato, S. *Bull. Chem. Soc. Jpn.* **2001**, *74*, 689.
(23) Sato, S.; Senga, T.; Kawasaki, M. *J. Phys. Chem. B* **1999**, *103*, 5063.
(24) Tolbert, M. A.; Middlebrook, A. M. *J. Geophys. Res.* **1990**, *95*, 22423.
(25) Stevenson, K. P.; Kimmel, G. A.; Dohnálek, Z.; Smith, R. S.; Kay, B. D. *Science* **1999**, *283*, 1505.
(26) Kimmel, G. A.; Stevenson, K. P.; Dohnálek, Z.; Smith, R. S.; Kay, B. D. *J. Chem. Phys.* **2001**, *114*, 5284.
(27) Kimmel, G. A.; Dohnálek, Z.; Stevenson, K. P.; Smith, R. S.; Kay, B. D. *J. Chem. Phys.* **2001**, *114*, 5295.
(28) Horn, A. B.; Koch, T.; Chester, M. A.; McCoustra, M. R. S.; Sodeau, J. R. *J. Phys. Chem.* **1994**, *98*, 946.
(29) Ataka, A.; Yotsuyanagi, T.; Osawa, M. *J. Phys. Chem.* **1996**, *100*, 10664.
(30) Sato, S., unpublished data.
(31) Bartram, M. E.; Koel, B. E. *Surf. Sci.* **1989**, *213*, 137.
(32) Bandow, H.; Akimoto, H.; Akiyama, S.; Tezuka, T. *Chem. Phys. Lett.* **1984**, *111*, 496.
(33) Fateley, W. G.; Bent, H. A.; Crawford, B., Jr. *J. Chem. Phys.* **1939**, *31*, 204.
(34) Hisatsune, I. C.; Devlin, J. P.; Wada, Y. *J. Chem. Phys.* **1960**, *33*, 714.
(35) Varetti, E. L.; Pimentel, G. C. *J. Chem. Phys.* **1971**, *55*, 3813.
(36) Givan, A.; Loewenschuss, A. *J. Chem. Phys.* **1989**, *90*, 6135.
(37) Givan, A.; Loewenschuss, A. *J. Chem. Phys.* **1989**, *91*, 5126.
(38) Greenler, R. G.; Rahn, R. R.; Schwartz, J. P. *J. Catal.* **1971**, *23*, 42.
(39) Zimmermann, F. M.; Ho, W. *Surf. Sci. Rep.* **1995**, *22*, 127.
(40) Zhou, X.-L.; Zhu, X.-Y.; White, J. M. *Surf. Sci. Rep.* **1991**, *13*, 73.
(41) Bass, A. M.; Ledford, A. E.; Laufer, A. H., Jr. *J. Res. Natl. Bur. Stand.* **1976**, *80*, 143.
(42) Kawasaki, M.; Kasatani, K.; Sato, H.; Shinohara, H.; Nishi, N. *Chem. Phys.* **1983**, *78*, 65.
(43) Gilton, T. L.; Dehnbostel, C.-P.; Cowin, J. P. *J. Chem. Phys.* **1989**, *91*, 1937.
(44) Harwood, M. H.; Jones, R. L. *J. Geophys. Res. D* **1994**, *99*, 22955.
(45) Wang, J.; Koel, B. E. *J. Phys. Chem.* **1998**, *102*, 8573.
(46) Goodman, A. L.; Underwood, G. M.; Grassian, B. H. *J. Phys. Chem.* **1999**, *103*, 7217.
(47) Barney, W. S.; Finlayson-Pitts, B. J. *J. Phys. Chem. A* **2000**, *104*, 171.
(48) Graham, J. D.; Robert, J. T. *J. Phys. Chem.* **1994**, *98*, 5974.
(49) Schaff, J. E.; Roberts, J. T. *J. Phys. Chem.* **1996**, *100*, 14151.
(50) Schaff, J. E.; Roberts, J. T. *Langmuir* **1998**, *14*, 1478.
(51) Sadtchenko, V.; Giese, C. F.; Gentry, W. R. *J. Phys. Chem. B* **2000**, *104*, 9421.